Inversion of TMI data for the magnetization vector using Gramian constraints

Yue Zhu, University of Utah, Michael S. Zhdanov, University of Utah, TechnoImaging and MIPT, and Martin Čuma, University of Utah and TechnoImaging

Summary

Conventional 3D magnetic inversion methods are based on the assumption that there is no remanent magnetization, and the inversion is run for magnetic susceptibility only. However, this approach ignores the situation where the direction of magnetization of the rocks is different from the direction of the induced magnetic field. This situation happens in a case of remanent magnetization, typical for geological structures such as kimberlites, dykes, iron-rich ultramafic pegmatitoids (IRUP), platinum group element (PGE) reefs, and banded iron formations (BIF). This paper presents a novel method of inversion of magnetic data for the scalar components of the magnetization vector. The method is based on a new magnetic forward modeling algorithm, which uses triangular prisms of arbitrary shape in order to achieve a more accurate approximation of the topography and complex geological structures. The inversion also includes Gramian constraints in order to obtain a robust solution of otherwise ill-posed magnetic inverse problems. The method was successfully tested on a number of synthetic models of the magnetized bodies. The results of inversion of airborne TMI data demonstrate how inversion for the magnetization vector with Gramian constraints can improve the subsurface imaging of kimberlites.

Introduction

Most 3D inversion methods in use today have been developed for recovering a 3D magnetic susceptibility model from the magnetic vector field, **H**, or from the total magnetic intensity (TMI) data, **T**, assuming that there is no remanent magnetization, that self-demagnetization effects are negligible, and that the magnetic susceptibility is isotropic (e.g., Li and Oldenburg, 1996, 2003; Portniaguine and Zhdanov, 2002; Zhdanov et al., 2011; Čuma et al., 2012). This implies that the magnetization is linearly proportional to the inducing magnetic field.

We should note, however, that, conventional susceptibility inversion ignores the effects of self-demagnetization, anisotropy, and remanent magnetization. To include both induced and remanent magnetization, we need to model on the magnetization vector rather than the scalar susceptibility. A variation of this approach was used by Lelièvre and Oldenburg (2009) to invert TMI data. This enables explicit inversion of the magnetization direction and amplitude, rather than just the magnetization amplitude only (e.g., Li et al., 2010). Recently, Ellis et al., (2012) reported further progress in the solution of this problem; they introduced a technique for regularized inversion for the magnetization vector. From the magnetization vector, one can recover information about both the remanent and induced magnetization. However, the practical difficulties of this inversion are related to the fact that, in this case one has to determine three unknown components of the magnetization vector within each cell instead of one unknown value of susceptibility, which increases practical nonuniqueness associated with this inverse problem.

In order to overcome these difficulties, we propose using a Gramian stabilizer in the framework of the regularized inversion for the magnetization vector, which was originally introduced by Zhdanov et al. (2012) for joint inversion of multimodal geophysical data. Another improvement in our forward modeling and inversion method is related to the use of an arbitrarily shaped triangular prism in order to gain a more accurate approximation of the topography and complex geological structures.

We use regularized inversion with focusing stabilization, as this recovers models with sharper boundaries and higher contrasts than regularized inversion with smooth stabilization does. The method is illustrated by synthetic model study and inversion of the TMI data collected in the Northwest Territories of Canada for kimberlite exploration.

Forward modeling of the magnetic fields using rectangular cells

The anomalous magnetic field induced by the magnetic source distributed within volume V with the magnetization vector $\mathbf{I}(\mathbf{r})$, can be represented by the following integral formula:

$$\Delta\mathbf{H}(\mathbf{r}') = \nabla' \iiint_V \mathbf{I}(\mathbf{r}) \left(\frac{1}{|\mathbf{r}-\mathbf{r}'|}\right) dv, \qquad (1)$$

where $\mathbf{r}$ is the radius vector of a point within the volume V; and $\mathbf{r}'$ is the vector of an observation point.

In order to include both induced and remanent magnetization, we represent the magnetization vector as follows:

$$\mathbf{I}(\mathbf{r}) = H_0\mathbf{M}(\mathbf{r}), \qquad (2)$$

where $\mathbf{M}$ has two parts: induced, $\mathbf{M}_{ind}$, and remnant, $\mathbf{M}_{rem}$, magnetizations, respectively:

$$\mathbf{M}(\mathbf{r}) = \mathbf{M}_{ind} + \mathbf{M}_{rem}. \qquad (3)$$

For modeling the magnetic data, we discretize the 3D earth model into a grid of N_m cells, each of constant magnetization vector.

One can compute the volume integral in equation (1) in closed form, as it was done in Bhattacharyya (1980) for magnetic susceptibility. We can also evaluate the volume integral numerically with sufficient accuracy using single

point Gaussian integration with pulse basis functions provided the depth to the center of the cell exceeds twice the dimension of the cell. In airborne magnetic surveys, the total magnetic intensity field is measured, which can be computed approximately using single point Gaussian integration as follows (Zhdanov, 2002):

$$\Delta T_k(\mathbf{r}') = \iiint_{V_k} f(\mathbf{r}-\mathbf{r}', \mathbf{M}_k)dv,$$

where

$$f(\mathbf{r}-\mathbf{r}', \mathbf{M}_k) = -H_0\mathbf{l}(\mathbf{r})\cdot\frac{1}{|\mathbf{r}-\mathbf{r}'|^3}\left[\mathbf{M}_k - \frac{3\big(\mathbf{M}_k\cdot(\mathbf{r}-\mathbf{r}')\big)(\mathbf{r}-\mathbf{r}')}{|\mathbf{r}-\mathbf{r}'|^2}\right], \quad (4)$$

and $\mathbf{M}_k = \big(M_{xk}, M_{yk}, M_{zk}\big)$ is the magnetization vector of the k^{th} cell

Forward modeling of the magnetic fields using triangular cells

The earth's surface is usually not flat and may have a variable topography. In order to accurately represent the surface undulation, one needs to use the cells with complicated shapes. To this end, we first split the k^{th} rectangular prism into four triangular prisms,

$$\Delta T_k(\mathbf{r}') = \sum_{j=1}^{4}\iiint_{V_k^{(j)}} f(\mathbf{r}-\mathbf{r}', \mathbf{M}_k)dv. \quad (5)$$

Using the concept of isoparametric elements developed in the theory of finite element methods (Jin, 2002), the volume integration in equation (5) can be accomplished by transforming an arbitrarily shaped triangular prism in the xyz-space into a regularly shaped element with straight sides and flat surfaces in the $\xi\eta\zeta$-space (Figure 1). This transformation can be expressed as follows:

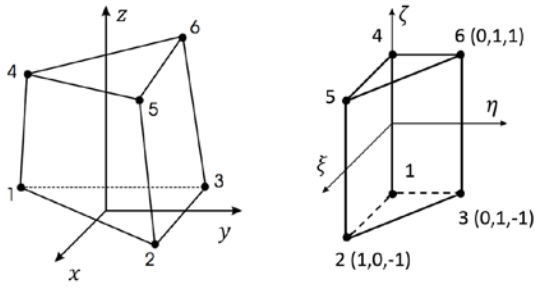

Figure 1: An arbitrarily shaped triangular prism in the xyz-space (left) and regularly shaped element with straight sides and flat surfaces in the $\xi\eta\zeta$-space (right).

$$x = \sum_{i=1}^{n_e} N_i^e(\xi,\eta,\zeta)x_i, \quad (6)$$

$$y = \sum_{i=1}^{n_e} N_i^e(\xi,\eta,\zeta)y_i, \quad (7)$$

$$z = \sum_{i=1}^{n_e} N_i^e(\xi,\eta,\zeta)z_i, \quad (8)$$

where n_e denotes the number of nodes within the element, $n_e = 6$ for triangular prism; (x_i, y_i, z_i) are coordinates of the i^{th} node of the triangular prism, which in turn depend on the j^{th} triangular prism and the k^{th} rectangular cell as follows:

$$N_i^e = \frac{1}{2}(1-\xi-\eta)(1+\zeta_i\zeta), i = 1, 4,$$
$$N_i^e = \frac{1}{2}\xi(1+\zeta_i\zeta), i = 2, 5,$$
$$N_i^e = \frac{1}{2}\eta(1+\zeta_i\zeta), i = 3, 6.$$

Now we can write the integral in equation (5) in the transformed $\xi\eta\zeta$-space,

$$\Delta T_k(x', y', z') = \sum_{j=1}^{4}\iiint_{V_k} f(\xi,\eta,\zeta,x',y',z',\mathbf{M}_k)dxdydz$$
$$= \sum_{j=1}^{4}\iiint_{\Delta} f^{(j,k)}(\xi,\eta,\zeta,x',y',z',\mathbf{M}_k)|J|d\xi d\eta d\zeta. \quad (9)$$

The term $|J|$ is the determinant of the Jacobian of the transformation described by expressions (6) to (8).

Following Martin et al. (2013), we use Gaussian quadrature to evaluate the integral over the regular triangular prism in the $\xi\eta\zeta$-space in equation (9):

$$\Delta T = \sum_{k=1}^{N_m}\Delta T_k =$$
$$\sum_{k=1}^{N_m}\sum_{j=1}^{4}\sum_{p=1}^{N_p} w_p f^{(j,k)}\big(\xi_p,\eta_p,\zeta_p,x',y',z',\mathbf{M}_k\big)|J|. \quad (10)$$

This approach can be extended to computing any potential field and/or its derivatives by simply changing the kernel function, f.

Using the discrete model parameters and discrete data, we can present the magnetic forward modeling, described by formula (10), as the following matrix operation:

$$\mathbf{d} = A\mathbf{m}, \quad (11)$$

where $\mathbf{d}$ is the N_d length vector of the observed total magnetic intensity field; $\mathbf{m}$ is the $3N_m$ length vector of the magnetization vector components; and A is a linear operator of the magnetic forward modeling problem.

Inversion of the TMI field for the magnetization vector

The inversion is based on minimization of the Tikhonov parametric functional (Zhdanov, 2002),

$$P^{\alpha}(\mathbf{m}) = \varphi(\mathbf{m}) + \alpha S_{MN,MS,MGS}(\mathbf{m}) \rightarrow \min, \quad (12)$$

where $\varphi(\mathbf{m})$ is a misfit functional:

$$\varphi(\mathbf{m}) = (W_d A\mathbf{m} - W_d\mathbf{d})^T(W_d A\mathbf{m} - W_d\mathbf{d}), \quad (13)$$

and W_d and W_m are the data and model weighting linear operators, respectively. The terms S_{MN}, S_{MS}, and S_{MGS} are the stabilizing functionals, based on minimum norm, minimum support, and minimum gradient support constraints, respectively. Minimization problem (12) can be solved using the re-weighted regularized conjugate gradient (RRCG) method (Zhdanov, 2002).

Inverting for the magnetization vector is a more challenging problem than inverting for scalar magnetic susceptibility, because we have three unknown values of the magnetization vector for every cell. We should notice that, there is inherent correlation between the different components of the magnetization vector. The different scalar components have similar spatial variations and represent the same zones of anomalous magnetization. Therefore, it is possible to expect that the different components of the magnetization vector should be mutually correlated. It was demonstrated in Zhdanov et al. (2012), that one can enforce the correlation between the different model parameters by using the Gramian constraints. Following the cited paper, we have included the Gramian constraint in equation (12) as follows:

$$P^{\alpha}(m) = \varphi(m) + \alpha c_1 S_{MN,MS,MGS}(m) + \alpha c_2 \sum_{\beta=x,y,z} S_G(m_\beta, \chi_{\text{eff}}). \quad (14)$$

where m is the $3N_m$ length vector of magnetization vector components; m_β is the N_m length vector of the β component of magnetization vector, $\beta = x, y, z$; χ_{eff} is the N_m length vector of the effective magnetic susceptibility, defined as the magnitude of the magnetization vector,

$$\chi_{\text{eff}} = \sqrt{M_x^2 + M_y^2 + M_z^2}; \quad (15)$$

and S_G is the Gramian constraint,

$$S_G(m_\beta, \chi_{\text{eff}}) = \begin{vmatrix} (m_\beta, m_\beta) & (m_\beta, \chi_{\text{eff}}) \\ (\chi_{\text{eff}}, m_\beta) & (\chi_{\text{eff}}, \chi_{\text{eff}}) \end{vmatrix}. \quad (16)$$

Using the Gramian constraint (16), we enhance a direct correlation between the scalar components of the magnetization vector with χ_{eff}, which is computed at the previous iteration of an inversion and is updated on every iteration. The advantage of using the Gramian constraint (16) is that it does not require any a priori information about the magnetization vector (e.g. direction, relationship between different components, and etc.).

Numerical model study -- a magnetized dipping dyke

We consider a model of a dipping dyke with a magnetization opposite to the inducing field. The dyke has a horizontal dimension of 250 m x 300 m and extends vertically from 50 m to 400 m as shown in Figure 2. The dyke has a constant magnetization with a magnitude of 0.06 SI. There are 441 receivers distributed over a 21 by 21 grid with a spacing of 50 m. The parameters of the inducing magnetic field were selected as follows: H_0 = 50 000 nT, $I = 75°$, and $D = 25°$.

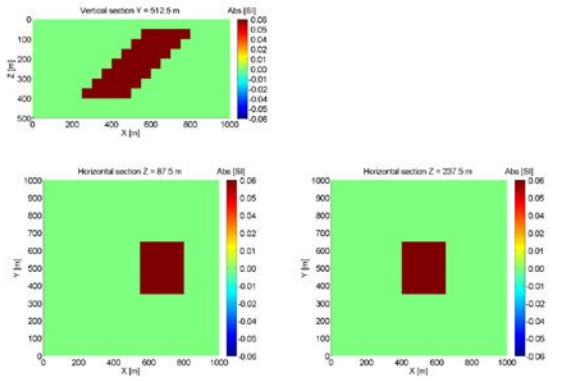

Figure 2: A model of the magnetized dipping dyke. The magnitude of magnetization f is 0.06 SI. The dyke has a horizontal dimension of 250 m x 300 m and extends from 50 m to 400 m in depth.

We invert for the magnetization vector using both TMI and magnetic components in three directions. The recovered magnetizations using only minimum norm stabilizer and using both minimum norm and Gramian constraint are shown in Figure 3. The different panels from the left to the right in this figure represent the scalar components, M_x, M_y, and M_z respectively. By using the Gramian constraint in the inversion, we are able to enhance the correlation between three components. The dipping structure is better resolved using our new approach. In this synthetic test, we also found artifacts associated with M_x and M_y components using only minimum norm stabilizer. These artifacts are greatly reduced in the inversion using both the minimum norm stabilizer and the Gramian constraint.

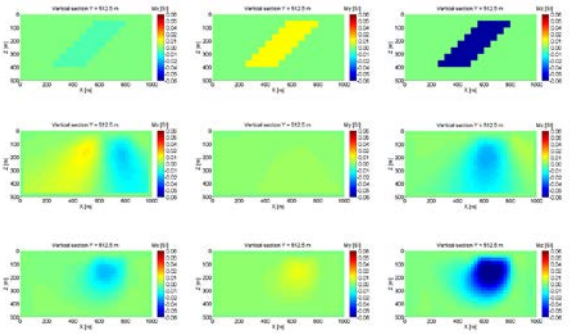

Figure 3: Vertical sections of the recovered scalar components of the magnetization vector obtained by the inversion based on the minimum norm stabilizer only (middle panels) and that based on both the minimum norm and Gramian constraints (bottom panel). The top panel shows the scalar components of the magnetization vector for the true model.

Inversion of TMI data for the magnetization vector using Gramian constraints

Case study

The area of the airborne magnetic survey is located in the Northwest Territories of Canada, which forms a distinct cratonic block within the Canadian Precambiran Shield. The kimberlites in this area have been characterized by strong remanent magnetization, which required the inversion for the magnetization vector instead of the scalar magnetic susceptibility. We have applied the developed inversion algorithm based on both minimum norm and Gramian constraints to the field airborne magnetic data collected in this area for kimberlite exploration. We have also taken into account the terrain heights in constructing the inversion domain. The typical magnetic susceptibility of kimberlites in the survey area is around 5×10^{-3} SI. We have expected to recover the targets associated with kimberlites with the magnitude of magnetization close to this number. The residual TMI anomaly within the airborne magnetic survey area was inverted for a magnetization vector using both the minimum norm and Gramian stabilizers. A set of triangular prisms was used to better represent the topography in the uppermost layer of the inversion domain.

Figure 4 shows vertical sections of the magnitude and scalar components of the magnetization vectors obtained by the inversion. Using both the minimum norm and Gramian stabilizers in the inversion, we were able to enhance a correlation between the different scalar components and recover a higher intensity of magnetization in the target area. Basically, the kimberlite deposits are associated with the round-shape anomalies having a negative M_z component. The elongated anomaly along the northeast and southwest directions are magnetic dykes, which extends deeper than the kimberlite pipes as seen from the vertical sections.

Figure 5 presents, for a comparison, the inversion results obtained by using the minimum norm stabilizer only. One can see the artifacts in the images of the M_x and M_y components in the locations of the kimberlite pipes. These artifacts were reduced by using the Gramian stabilizer in the inversion.

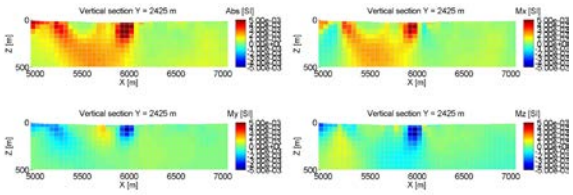

Figure 4: Vertical sections of the recovered magnitude and scalar components of the magnetization vector in the survey area. Both the minimum norm and Gramian stabilizers were used in the inversion.

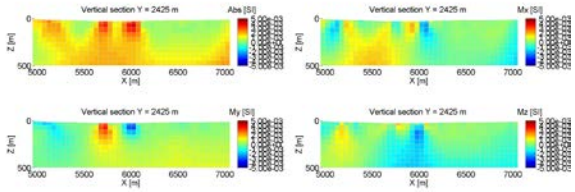

Figure 5: Vertical sections of the recovered magnitude and scalar components of magnetization vector obtained by the inversion with the minimum norm stabilizer only. One can see the artifacts in the images of the M_x and M_y components in the locations of kimberlite pipes.

Conclusions

A majority of the conventional 3D magnetic inversion methods are based on the assumption that there is no remanent magnetization and the inversion is applied to determine the subsurface distribution of a scalar magnetic susceptibility. However, in many geological areas the direction of magnetization in a rock differs from the direction of the inducing magnetic field, which is manifested by the presence of remanent magnetization in the rocks. In this case, the inversion should be applied for the magnetization vector rather than the scalar susceptibility.

We have developed a novel method of inversion of the total magnetic intensity (TMI) data for the scalar components of the magnetization vector. This method is based on a new magnetic forward modeling algorithm, which uses triangular prisms of arbitrary shape in order to achieve a more accurate approximation of the topography and complex geological structures. The inversion also includes Gramian constraints in order to obtain a robust solution of otherwise ill-posed magnetic inverse problems.

The method was successfully illustrated by a number of synthetic models of the magnetized bodies. The results of inversion of airborne TMI data demonstrate how inversion for the magnetization vector with Gramian constraints can improve the subsurface imaging of kimberlites.

Acknowledgement

The authors acknowledge CEMI and TechnoImaging for support of this research. We are also thankful to the Center for High Performance Computing, University of Utah, for providing computational resources. The authors also acknowledge Rio Tinto for providing the data.

References

Bhattacharyya, B. K., 1980, A generalized multibody model for inversion of magnetic anomalies: Geophysics, **29**, 517-531. doi: 10.1190/1.1441081.

Čuma, M., G. Wilson, and M. S. Zhdanov, 2012, Large-scale 3D inversion of potential field data: Geophysical Prospecting, **1**(14), doi: 10.1111/j.1365-2478.2011.01052.

Ellis, R. G., B. De Wet, and I. N. Macleod, 2012, Inversion of magnetic data from remanent and induced sources: 22nd International Geophysical Conference and Exhibition, ASEG, Expanded Abstracts, 1-4.

Jin, J., 2002, Finite element method in electromagnetics: Wiley-IEEE Press.

Lelièvre, P. G., and D. W. Oldenburg, 2009, A 3D total magnetization inversion applicable when significant, complicated remanence is present: Geophysics, **74**, L21-L30, doi: 10.1190/1.3103249.

Li Y. and D. W. Oldenburg, 1996, 3-D inversion of magnetic data: Geophysics, **61**, 394-408. doi: 10.1190/1.1443968.

Li Y. and D. W. Oldenburg, 2003, Fast inversion of large-scale magnetic data using wavelet transforms and a logarithmic barrier method: Geophysical Journal International, **152**, 251-265. doi: 10.1046/j.1365-246X.2003.01766.

Li, Y., S. E. Shearer, M. M. Haney, and N. Dannemiller, 2010, Comprehensive approaches to 3D inversion of magnetic data affected by remanent magnetization: Geophysics, **75**, L1-L11. doi: 10.1190/1.3294766.

Martin, R., V. Monteiller, D. Komatitsch, S. Perrouty, M. Jessell, S. Bonvalot and M. Lindsay, 2013, Gravity inversion using wavelet-based compression on parallel hybrid CPU/GPU systems: application to southwest Ghana: Geophysical Journal International, **195** (3), 1594-1619, doi: 10.1093/gji/ggt334.

Portniaguine O. and M. S. Zhdanov, 2002, 3-D magnetic inversion with data compression and image focusing: Geophysics, **67**, 1532-1541. doi: 10.1190/1.1512749.

Zhdanov, M. S, 2002, Geophysical inverse theory and regularization problems: Elsevier.

Zhdanov, M. S., X. Liu, G. A. Wilson, and L. Wan, 2011, 3D migration for rapid imaging of total-magnetic-intensity data: Geophysics, **77**(2), J1-J5, doi: 10.1190/GEO2011-0425.1.

Zhdanov, M. S., A. V. Gribenko, and G. Wilson, 2012, Generalized joint inversion of multimodal geophysical data using Gramian constraints: Geophysical Research Letters, **39**, L09301, 1-7.